Subpicosecond resolution studies of the $H+CO_2 \rightarrow CO+OH$ reaction photoinitiated in CO_2–HI complexes

S. I. Ionov, G. A. Brucker,[a] C. Jaques, L. Valachovic, and C. Wittig
Department of Chemistry, University of Southern California, Los Angeles, California 90089

(Received 6 July 1993; accepted 22 July 1993)

Time resolved studies of the title reaction have been carried out by photodissociating the HI moiety within weakly bound CO_2–HI complexes. The $HOCO^{\dagger}$ intermediate decomposes via a unimolecular decomposition mechanism, and the emerging hydroxyl radicals are monitored with subpicosecond temporal resolution by using laser-induced fluorescence. The measured rates are in good agreement with several theoretical predictions: Rice, Ramsperger, Kassel, and Marcus (RRKM) calculations; classical trajectory simulations on the best available potential energy surface; and recent quantum scattering calculations.

I. INTRODUCTION

Because of its relevance to the fields of atmospheric chemistry[1–3] and combustion,[4,5] many aspects of reaction (1) have been examined in detail by both experimentalists and theorists. This system occupies a special place in the area of the kinetics and dynamics of small prototypical reactive systems:

$$CO+OH \rightleftarrows H+CO_2, \quad \Delta H=-25.6 \text{ kcal mol}^{-1}. \quad (1)$$

Temperature dependent rate constants have been measured with almost unparalleled accuracy,[6–11] and they have been shown to display an intriguing behavior, i.e., $k_1(T)$ is nearly constant at low temperatures and increases above 500 K. This variation has been attributed to the participation of the vibrationally excited $HOCO^{\dagger}$ intermediate, which decomposes via a unimolecular decomposition mechanism:

$$HOCO^{\dagger} \rightarrow CO+OH \quad (2a)$$

$$\rightarrow H+CO_2. \quad (2b)$$

Additionally, the HOCO species has been successfully isolated in inert, cryogenic matrices,[12(a)] and its IR spectrum suggests a hydroxyformyl structure with nearly isoenergetic *cis* and *trans* isomers. Very recent spectroscopic studies of gas phase HOCO have confirmed the matrix results and have provided a number of useful molecular constants.[12(b)–12(d)]

Perhaps the most complete modeling of the kinetics of reactions (1) and (2) has been that of Brunning *et al.*[10] These authors reproduced the temperature and isotope dependences of k_1 by using transition state theory with parameters based mainly on *ab initio* calculations.[13] Later, the same group conducted measurements over a temperature range extending down to 82 K.[11] This study demonstrated a negligible temperature dependence of $k_1(T)$ between 300 and 82 K and resulted in further fine tuning of the entrance channel barrier. Although the presently accepted transition state frequencies and reaction barriers are not the last word, it is probably safe to assume that the overall view of reactions (1) and (2) is robust. An energy diagram is given in Fig. 1.

Different aspects of $H+CO_2$ collisional dynamics have been explored by using photolytic sources of nearly monoenergetic hydrogen atoms.[14–25] Oldershaw and Porter determined the threshold for the $H+CO_2$ reaction more than two decades ago;[14] Tomalesky and Sturm studied reaction probabilities of fast hydrogen atoms with CO_2;[15] Quick, Weston, and Flynn characterized vibrational excitation of CO_2 in collisions with fast hydrogen atoms;[16] Wittig and co-workers measured the kinetic energy dependence of the relative reaction cross sections,[17] and noted somewhat nonstatistical OH V, R, T distributions.[18] OH rotational distributions deriving from the above reactions were also reported by Wolfrum and co-workers, particularly Kleinermanns.[19–22] Furthermore, these authors estimated the overall reaction cross section to be 4 Å^2 at a collision energy of 20 970 cm^{-1}.[23] Energy partitioning into the CO rotational and vibrational degrees of freedom has been studied by infrared diode laser kinetic absorption spectroscopy[24] and by VUV laser-induced fluorescence (LIF).[25] Minor controversies notwithstanding, these studies provide a comprehensive view of the disposal of the available energy amongst the CO and OH degrees of freedom.[26]

Subtle details of reactions (1) and (2) were obtained from studies of the corresponding photoinitiated reactions in CO_2–HX complexes, where X=Cl, Br, or I.[26] Chemical transformations were initiated by photolyzing the HX moiety within the complex. The liberated hydrogen atom attacks CO_2 with a respectable amount of translational energy, yielding OH and CO. Capitalizing on the qualitatively different structures of CO_2–HCl vs CO_2–HBr (the former being quasilinear with hydrogen pointing towards oxygen, whereas the latter is inertially T shaped with bromine facing the carbon),[26–31] Shin *et al.* observed at least an order of magnitude enhancement in the reaction probability for broadside versus end-on hydrogen attack.[26,30,32] State resolved studies of OH produced from CO_2–HI and CO_2–HBr complexes revealed rotational distributions that are somewhat colder than those obtained in the corresponding single collision gas phase reactions. The

[a]Present address: Stanford Research Systems, 1290D Reamwood Ave., Sunnyvale, California 94089.

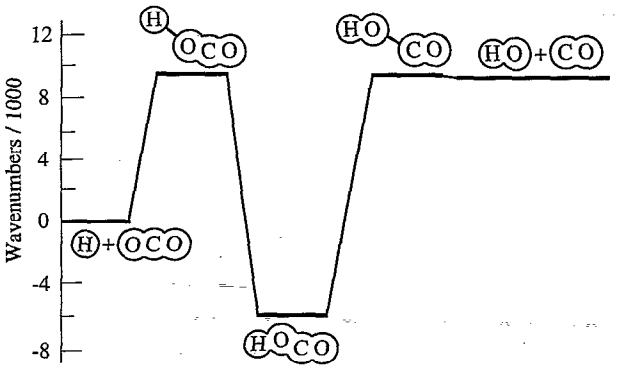

FIG. 1. Schematic drawing of the $H+CO_2 \rightleftarrows HOCO^{\dagger} \rightleftarrows OH+CO$ reaction path (Ref. 13).

differences can be rationalized, at least in part, by the squeezed atom effect.[30,33] This accounts for the simultaneous repulsion between CO_2, H, and I that occurs during the course of HI photodissociation and concomitant HOCO formation. Relative to the corresponding gas phase reaction, this leads to higher I—HOCO center-of-mass (c.m.) translational energies and, consequently, lower vibrational excitations of the $HOCO^{\dagger}$ intermediate. In turn, the lower $HOCO^{\dagger}$ excitations account for the colder product rotations.

When conclusions about reactions (1) and (2) are drawn from the corresponding photoinitiated reactions in weakly bound complexes, concerns arise regarding the role of the departing halogen atom. Is it really a spectator, or is its presence important to the reaction dynamics? Does CO_2–HX photochemistry proceed through a "supramolecule," such as OC(X)OH, characterized by established chemical bonds? Although definitive answers have not yet been obtained, it is worthwhile to draw upon recent *ab initio* calculations for CO_2–HBr.[34] These suggest that the main chemical effect in photoinitiating the reaction within the complex is steric; i.e., there is no significant propensity for carbon-bromine bonding for either the A' or A'' orientation of the unpaired halogen orbital. These observations suggest that reaction proceeds through the $HOCO^{\dagger}$ intermediate, as in the gas phase.

In a seminal experiment, Scherer *et al.*[35,36] observed reaction (2) in the time domain by photoexciting CO_2–HI complexes and probing OH products with laser pulses of several picoseconds duration. They reported OH buildup times in the picosecond range, confirming that $HOCO^{\dagger}$ intermediates decay via a unimolecular decomposition mechanism. These studies paved the way to probing the time evolution of a number of small prototypical reactive systems.

$HOCO^{\dagger}$ lifetimes have also been probed, albeit indirectly, in very recent crossed molecular beams studies.[37] Anisotropic c.m. translational energy distributions suggested that $HOCO^{\dagger}$ lifetimes might be shorter than those reported earlier.[35,36] Since the time resolved measurements involved the use of CO_2–HI complexes, whereas the crossed beams studies made use of single collisions between CO and OH, comparisons require care. For example, uncertainties derive from the presence of the iodine atom and/or higher-than-binary clusters in the time resolved studies, and from reliance on a qualitative model to interpret the results of the molecular beams studies.

A global potential energy surface has been obtained by matching scaled *ab initio* calculations in the vicinity of all the saddle points and minima, and smoothly interpolating in between.[13] Detailed quasiclassical trajectory studies conducted on this surface have demonstrated that reaction proceeds, as expected, via the $HOCO^{\dagger}$ intermediate.[38] $HOCO^{\dagger}$ is formed when hydrogen approaches CO_2 broadside near an oxygen atom, which is consistent with the experimental results on the reaction stereospecificity. $HOCO^{\dagger}$ decays, for the most part, via a unimolecular decay mechanism, yielding both $CO+OH$ and $H+CO_2$, with the former channel dominating over the latter. Although the potential energy surface is not perfect, e.g., its HO–CO transition state is thought to be too loose,[38] the trajectory simulations give rise to qualitative and sometimes even quantitative agreement with experimental data on reaction cross sections, product energy partitioning, and thermal and state resolved rate constants. The same calculations have yielded shorter $HOCO^{\dagger}$ lifetimes than those reported by Scherer *et al.*[35,36] RRKM calculations that use transition state frequencies obtained from *ab initio* calculations or by fitting $k(T)$ over the range 300–2000 K give results that are in general agreement with the trajectory studies (i.e., within a factor of 2).

The present paper is a full description of our experimental studies of the photoinitiated reaction: CO_2–HI $+h\nu \rightarrow CO+OH+I$, using the subpicosecond resolution pump–probe method to monitor OH buildup.[35,36] A preliminary report was published earlier.[39] Effects due to coherence are minimized in an attempt to obtain results that can be compared directly to reaction rates. We observe shorter OH buildup times than those reported by Scherer *et al.*, whose measurements differ from ours in several respects.[35,36] A detailed comparison of the results from the two experiments will be presented later.[40] Although the overall photoinitiated reaction involves five atoms, our measured rates agree with a mechanism in which $HOCO^{\dagger}$ is formed with nearly the energy of its single collision counterpart and then decomposes as per RRKM theory. The rates are also in general agreement with the trajectory calculations of Schatz and co-workers[38] and recent quantum scattering calculations of Clary and co-workers.[41]

II. EXPERIMENT

The experimental apparatus is similar to that used in our previous work,[42] so only essential details are presented. Measurements are carried out in a vacuum chamber equipped with a supersonic expansion source (piezoelectric pulsed nozzle; 250 μs duration, 0.25 mm$\times$1 mm slit), a quadrupole mass spectrometer, a Hamamatsu 943-02 PMT, and collecting optics for LIF measurements (Fig. 2). The base pressure in the chamber is 10^{-6} Torr; operating pressures are $\sim 10^{-4}$ Torr when the nozzle is firing. CO_2–HI complexes are formed by expanding mixtures of

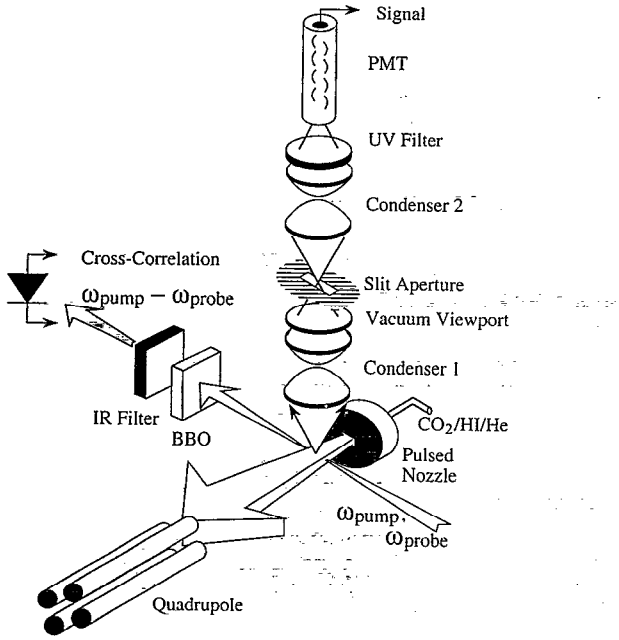

FIG. 2. Experimental arrangement, showing co-propagating pump and probe subpicosecond beams, supersonic pulsed slit expansion, a quadrupole mass spectrometer, and LIF collection optics. Not shown are input and output quartz windows mounted 55 cm from the jet axis at the Brewster angle and baffles for suppressing scattered light.

2% HI, 3% CO_2, and 95% He through the nozzle at a total stagnation pressure of 2.3 atm. Mixtures are prepared in a gas handling system and are kept in a stainless-steel cylinder. Before entering the nozzle, mixtures are passed through a cold trap maintained at −90.6 °C (heptane slush) that purifies the gas by removing I_2 without freezing CO_2 and HI. The beam composition is monitored by the quadrupole mass spectrometer located on the beam line across the chamber. Under the present conditions, $(CO_2)_2HI^+$ and $CO_2(HI)_2^+$ ion signals are less than 15% of that from CO_2HI^+.

Reactions in complexes are initiated and probed with subpicosecond laser pulses, which are generated as shown in Fig. 3. The primary source of tunable subpicosecond radiation is a dual-jet dye laser (Coherent 702-1) synchronously pumped at 76 MHz by the second harmonic of an actively mode-locked Nd:YAG laser (Spectron SL 903). Typically, 18 W is obtained at 1064 nm and 1.8 W is obtained at 532 nm after frequency doubling in a LBO crystal. The dye laser operates on Kiton Red and DQTCI as the gain and saturable absorber dyes, respectively, generating a train of 500 fs pulses at 618.2 nm. Although 250 mW average power is typically available at the output of the dye laser, only ~100 mW is used to avoid pulse broadening.

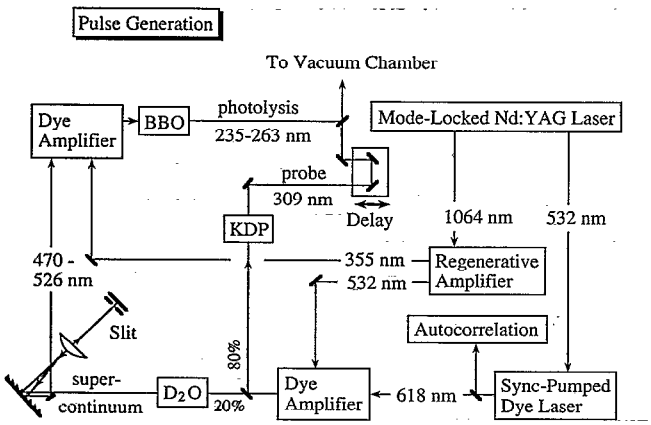

FIG. 3. Block diagram of the subpicosecond resolution laser system.

Dye laser pulses are amplified in a three-stage dye amplifier (Continuum PTA-60) pumped by the second harmonic of a Nd:YAG regenerative amplifier (RGA). The RGA amplifies pulses from the mode-locked Nd:YAG laser, and its output is synchronized with the dye laser train. Normally, 35 mJ (532 nm) and 45 mJ (355 nm) pulses are obtained after, respectively, frequency doubling and tripling; the pulse duration is ~70 ps. The dye amplifier operates on a Sulforhodamine 640/water solution; typically, 0.5 mJ pulses are obtained at 618.2 nm. This radiation is divided into two beams by a broadband beam splitter. The first beam, containing ~80% of the energy, is frequency doubled in a KDP crystal producing 40–100 μJ, 500 fs pulses at 309.1 nm. The bandwidth of this radiation is ~80 cm^{-1}, which is 4 times the transform limit. The 309.1 nm pulses are used to probe OH products by exciting LIF in the $A\,^2\Sigma \leftarrow X\,^2\Pi$ system. The spectral width of the probe is broad enough to excite OH in various rotational states from $N=2$ to 20 with $\langle N \rangle \sim 5.5$.

The remaining 20% of the amplified radiation is focused by 10 cm focal length (f.l.) lens into a D_2O cell producing a subpicosecond continuum. This white light is recollimated by a 8 cm f.l. lens and passed through a Glan–Taylor cube polarizer that selects vertical polarization. A desired wavelength in the range 470–526 nm is spectrally filtered from the white continuum in a chirp-compensated monochromator.[36,43] Briefly, the monochromator consists of a 1800 grooves/mm grating, a 15 cm f.l. cylindrical lens, a slit, and a mirror. The white light is dispersed by the grating in the horizontal plane and focused by the lens onto a vertically oriented slit that selects the required spectral interval. The slit is directly followed by a mirror reflecting the selected portion of the white light back to the grating; as a result, the pulse stretching introduced during the first pass is compressed by the second reflection. The mirror is tilted slightly, so that the outgoing beam propagates ~2 cm below the incoming one. When the distance between the grating and the lens is equal to its focal length, the monochromator has zero group velocity dispersion.[43] Essentially no pulse broadening of spectrally selected pulses is observed for slit openings larger than 0.6 mm.

Spectrally selected 470–526 nm pulses are amplified in a two-stage dye amplifier pumped by the RGA third harmonic. The amplifier is similar to that described in Ref. 44. The first stage is transversely pumped by ~10% of the available power; the remaining pump radiation is used for the second stage, which is a prism cell with a 3 mm diameter dye channel. Coumarin 480 and 503 laser dyes are

used for wavelengths below and above 480 nm, respectively; dye concentrations in each stage are adjusted individually for maximum power and minimal pulse broadening. Depending on the wavelength, the amplifier delivers 0.3–1 mJ pulses with no significant temporal broadening. The amplified beam is frequency doubled in a 150 μm long BBO crystal; the resulting 235–263 nm pulses are used for photodissociating HI. The bandwidth of the pump pulses is close to that of the probe, 80 cm^{-1}.

After passing through a computer-controlled delay stage (Aerotech ATS100), the probe beam is combined with the pump on a dichroic mirror and focused into the supersonic jet 5 mm downstream from the nozzle. Both beams are horizontally polarized. Since the pump and probe radiations have different divergences, independent focusing is used to optimize their spatial overlap in the focal plane. In practice, 1 m and 2 m f.l. lenses are employed for the pump and probe beams, respectively. Fluorescence from laser excited OH radicals is collected at 90° by an F/1 quartz condenser. One photon per laser shot is considered a respectable signal; for that reason, special precautions are taken to reduce scattered light on the PMT. First, entrance and exit windows are mounted at the Brewster angle 55 cm from the jet; a set of baffles is positioned between the windows and the jet; a Schott UG11 filter with a 250–390 nm transmission window is placed in front of the PMT to block scattered pump radiation; and, finally, LIF is spatially filtered by a 5 mm×25 mm slit oriented along the laser beams in the focal plane of the first condenser (Fig. 2). Fluorescence passing through the slit is picked up by another F/1 condenser and focused onto the entrance window of the PMT.

The PMT signals are preamplified, digitized and stored in a computer that counts photons within the 70–1200 ns interval after laser firing. Pump–probe cross correlations are obtained simultaneously by difference frequency generation in a 100 μm BBO crystal. For that purpose, the co-propagating UV beams are focused by a 5 cm f.l. lens, and the emerging 1–1.7 μm difference frequency radiation is separated from the UV by a Corion LG-790 long-pass filter and focused onto a Ge photodiode. At the longest pump wavelength, 263 nm, the difference frequency, 1.76 μm, is close to the detector cutoff, and therefore the cross correlation signals are weak. Under these conditions, cross correlations are obtained by using UV photolysis of H_2O_2, as discussed later.

III. EXPERIMENTAL RESULTS

Representative LIF traces and the corresponding cross correlations are presented in Fig. 4 for λ_{pump} values in the range 235–263 nm and for λ_{probe} set at 309.1 nm. Each scan is acquired over periods ranging from 1–4 h, depending on the magnitude of the signal. As seen from Fig. 4, LIF signals appear when the pump pulse precedes the probe pulse and they go down to the background level when the probe precedes the pump. No such transient signals are observed when the probe laser is detuned from the OH $A\,^2\Sigma \leftarrow X\,^2\Pi$ system (i.e., to $\lambda_{probe}=304$ nm), as expected. In accord with the energy dependence of the reaction cross

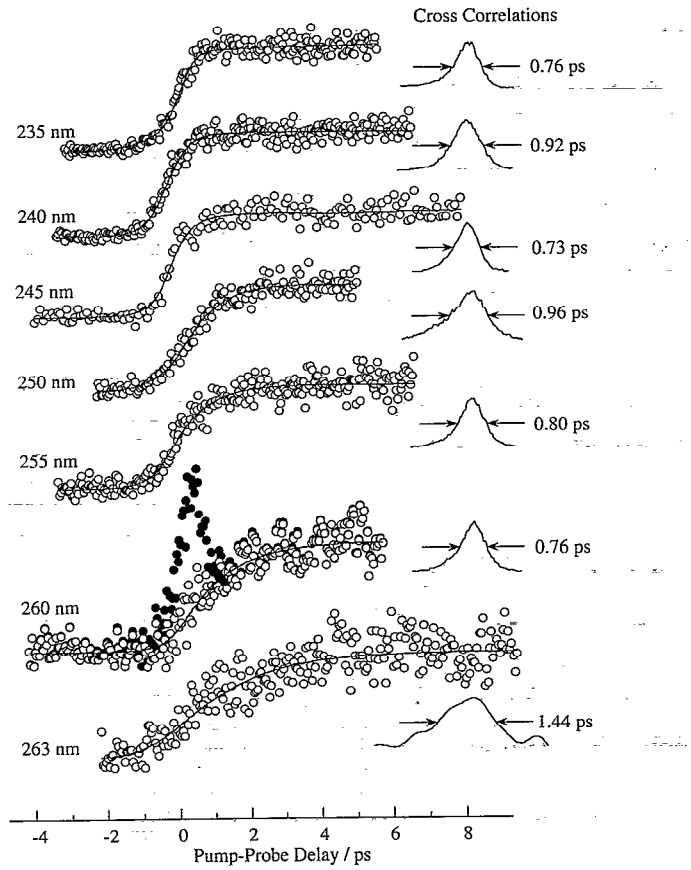

FIG. 4. Representative scans of LIF photon counts vs pump–probe delay for the CO_2–HI→CO+OH+I reaction; $\lambda_{probe}=309.1$ nm; pump wavelengths are indicated. The spurious peak at $\Delta t \sim 0$ for $\lambda_{pump}=260$ nm is believed to be due to two-photon excitation of HI (see Fig. 5 and the text). For this wavelength, both the original and the "corrected" data are presented. Also shown are the corresponding cross correlations obtained by difference frequency generation in a BBO crystal. For $\lambda_{pump}=263$ nm, the cross correlation is obtained by differentiating the hydrogen peroxide signals (the bottom curve in Fig. 7). Solid lines are least-squares fits of the experimental data to Eq. (3).

section,[17] the signal decreases from ~2 photons per shot at $\lambda_{pump}=235$–240 nm to ~0.3 photons per shot at 263 nm. The signal at 263 nm is so low that no attempt was made to study the reaction at longer photolysis wavelengths.

No LIF signals were observed at photolysis wavelengths below 255 nm when using expansion cooled HI/He mixtures, i.e., without CO_2. However, a distinct peak is seen clearly with HI/He mixtures at zero delay for $\lambda_{pump}=260$ nm. An identical peak is seen in the CO_2–HI scan at 260 nm, as shown in Fig. 4. Moreover, similar (but barely detectable) peaks are observed for CO_2-free mixtures at λ_{pump} values of 263 and 255 nm. This spurious LIF signal may be due to two-color, two-photon absorption of HI. This is consistent with the LIF signals being proportional to the overlap between the pump and probe pulses, i.e., to their cross correlation. Figure 5 depicts the likely HI levels involved; however, a lack of adequate spectroscopic information[45] precludes the possibility of a definitive assignment. In our data analyses, the spurious transient at $\lambda_{pump}=260$ nm is accounted for by subtracting weighted cross

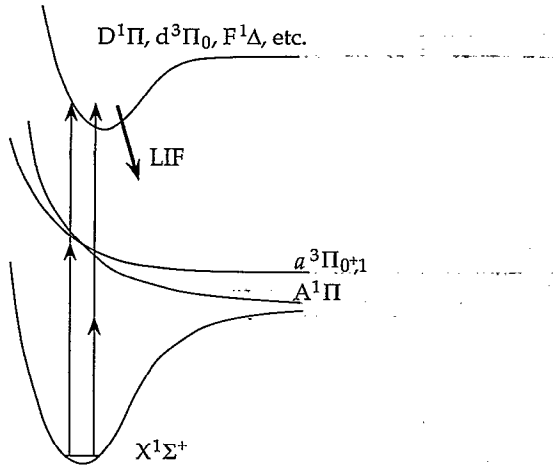

FIG. 5. HI levels that might be involved in the spurious two-photon LIF at $\lambda_{pump}=260$ nm.

correlations from the corresponding LIF signals (see Fig. 4). No correction is required at any other wavelength.

Figure 6 shows the correlation between the OH LIF and the CO_2HI^+ mass spectrometer signals. The different data points were obtained by varying the CO_2 percentage 0%–3% while maintaining other conditions constant, such as [HI]/[He] ratio, the backing pressure, and the laser energies. These measurements show a linear relationship between the amplitudes of the OH LIF and the CO_2HI^+ mass spectrometer signals, especially at low ion signals. From this, it is tempting to assume that our pump–probe signals originate solely from binary CO_2–HI complexes. However, the results are not conclusive, since CO_2HI^+ ions may derive at least in part from larger clusters upon electron impact ionization. Indeed, the LIF signal amplitude versus $[CO_2HI^+]$ tends to saturate at higher CO_2 partial pressures, where $[(CO_2)_2HI^+]$ and $[CO_2(HI)_2^+]$ increase substantially. Furthermore, whereas $[CO_2HI^+]$ is larger for very concentrated mixtures (e.g., $HI/CO_2/He = 0.05/0.1/0.85$ results in $[CO_2HI^+]/[(CO_2)_2HI^+]/[CO_2(HI)_2^+] = 1/0.6/0.2$, respectively), the corresponding LIF signals are smaller. This suggests that the photoinitiated reactions may be inhibited in larger clusters, in the sense that a gas phase OH product is not produced.

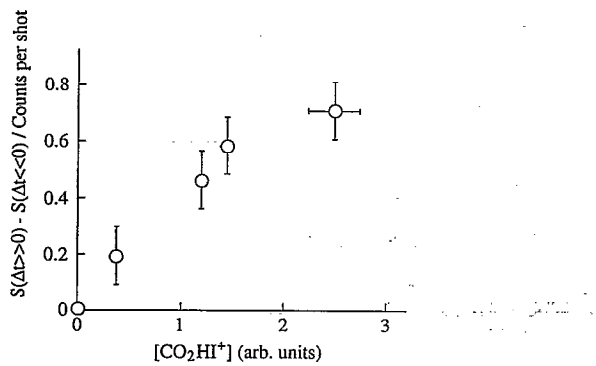

FIG. 6. OH LIF signal intensity versus CO_2HI^+ mass spectrometer signal intensity.

Another argument in favor of reaction inhibition in larger clusters comes from the time resolved measurements. We had anticipated different (i.e., slower) reaction rates for expansions having an abundance of higher-than-binary clusters. To our surprise, we found that, within the experimental uncertainty, the OH risetimes were independent of the $HI/CO_2/He$ ratios. Keeping in mind the distinction between proven and likely, we offer the following statement: The observed OH LIF signals originate from photoinitiated reactions in weakly bound complexes which are *predominantly* CO_2–HI.

As a control experiment, we recorded traces for the time resolved photodissociation of H_2O_2 in a gas flow with the same pump and probe laser pulses. With $\lambda_{pump} \leqslant 300$ nm, H_2O_2 is excited to a repulsive potential[46] and dissociates on the time scale of a vibrational period. Consequently, OH radicals are produced instantaneously at our present temporal resolution. Figure 7 presents characteristic signals for H_2O_2 photodissociation. Analog averaging is used because the signals are too large for photon counting.

IV. DISCUSSION

A. Extracting reaction rates

As seen in Fig. 4, the experimentally determined OH appearance rates decrease when the pump photon energy decreases, with the characteristic reaction times noticeably exceeding the cross correlation widths for $\lambda_{pump} \geqslant 260$ nm. However, for the most part, reaction proceeds on the same general time scale as the cross correlations. This makes deconvolution a challenge. Recently, there have been extensive discussions (even controversy) on the recovery of molecular dynamics information from the time resolved pump–probe studies of photodissociation.[47–51] Coherent effects may need to be taken into explicit account in analyses, and since our pump–probe studies are not immune from such complications, we shall begin with a brief overview of coherent effects in pump–probe experiments. We first emphasize photodissociation on repulsive surfaces (as probed by LIF) and then extend the arguments to cover the present system.

Three potential surfaces are involved in a typical photodissociation experiment: the ground surface; a repulsive surface leading to ground state products; and a higher surface associated with the transitions involved in LIF. A pump pulse takes molecules from the ground to the first repulsive surface, and the outcome is monitored via LIF, which is excited by a suitably delayed probe pulse. As stated earlier, in most of the measurements reported here, photoinitiated reaction proceeds on the same general time scale as the durations of the laser pulses. Under these conditions, the population on the upper potential surface, which gives rise to the measured fluorescence, is comprised of many partial waves launched by different portions of the pump and probe pulses. As a result, the LIF signal may reflect constructive and destructive interferences between the partial waves. This has been clearly demonstrated by

Williams and Imre, who applied wave-packet propagation techniques to ICN photodissociation.[47] Further developments were made by Krause, Shapiro, and Bersohn for Gaussian pulses.[48] These authors expressed the LIF signal as a coherent superposition of a "molecular" part, i.e., a product wave function in the vicinity of the equilibrium configuration, and a part representing products in the asymptotic limit. Other coherent effects come into play when product rotations are taken into account.[49]

Two essential requirements must be satisfied to observe interferences in pump–probe experiments. Firstly, the laser-excited partial waves must be reproducible from one shot to another. In practice, this is achieved by using coherent, transform limited pulses with reproducible time envelopes. Such pulses obey a relationship between their duration, Δt, and spectral width, $\Delta\omega$. For example, Gaussian and sech^2 envelopes give $\Delta t \times \Delta\omega = 0.44$ and 0.315, respectively, for full width at half maximum (FWHM) values of Δt and $\Delta\omega$. As discussed earlier, the spectral widths of our pulses are 4 times the transform limit. The time envelopes for such broadband radiation resemble noise with correlation time $\sim 1/\Delta\omega$. Moreover, these noise features are not reproducible from one shot to the next due to incomplete synchronization of the dye laser modes. The partial waves created by uncorrelated portions of the light pulses interfere with each other so that they only contribute individually; i.e., the cross terms cancel. In this case, classical rate equations describe excitation; similar arguments apply to probing.

Secondly, for coherence to play a role in our measurements, the dynamics must be "regular." In classical mechanics, this refers to reactions proceeding along a well-defined path, as in the case of bond rupture on a repulsive potential surface. Quasiclassically, regular dynamics implies nearly identical phase shifts for trajectories of close origins. As opposed to regular dynamics, reactions involving long-lived intermediates generally display chaotic dynamics, i.e., their trajectories sample the available phase space randomly. In such systems, phase shifts vary randomly for different trajectories, so the cross terms for the corresponding partial waves cancel, and the total signal is a sum of the individual partial wave contributions. Therefore, the evolution of long-lived intermediates is expected to follow rate equations. We note that trajectory simulations of reaction (1) indicate a long-lived (i.e., as compared to the time scale of vibrations) $HOCO^{\dagger}$ intermediate.[38] A similar mechanism is deemed likely for photoinitiated reactions in CO_2–HI complexes.[26]

Felker and Zewail[52–54] have discovered a different type of coherence that is observed when aligned species are produced promptly by pump radiation. Such species comprise a wave packet of many rotational states, each evolving as $\exp(-i\omega_J t)$. As a result of different evolutions, the original orientation is quickly scrambled. However, at $t_n = n\pi/B$ each rotational state acquires a phase shift of $n\pi J(J+1)$, which is proportional to an integer times 2π, and therefore initial alignment is restored. In turn, this recovered distribution is lost and then regained again at t_{n+1}. When probed by properly polarized light, aligned products give rise to higher LIF signals than scrambled ones, resulting in a series of peaks separated by π/B. Rigorous treatments predict additional features.[49,52–54]

Our linearly polarized pump pulses align HI molecules as per their transition moment. As seen from the data presented in Fig. 4, the CO_2–$HI + h\nu \rightarrow CO + OH + I$ reaction rates are probably faster than HOCO rotational periods. Under these conditions, the production of aligned OH products is possible if (i) the hydrogen atom is well localized within the CO_2–HI reference frame, and (ii) the $HOCO \rightarrow CO + OH$ transition state is sufficiently rigid. We tried to find rotational recurrences by varying the pump–probe delays over a 40 μs range. No recurrences were found, suggesting that OH is produced with scrambled orientation.

In summary, the aforementioned qualitative discussion suggests that coherent effects are of minor importance for the present experimental conditions. Consequently, rate equations are applicable to excitation, chemical evolution, and subsequent probing of the photoinitiated reaction. Thus, the signal $S(t)$ is given by

$$S(t) = \text{const} \times \int_{-\infty}^{t} ds\, R_I(s) N(t-s), \tag{3}$$

where

$$R_I(s) = \int_{-\infty}^{\infty} d\tau I_{\text{pump}}(\tau) I_{\text{probe}}(\tau - s) \tag{4}$$

is an intensity cross correlation, $I_{\text{pump}}(t)$ and $I_{\text{probe}}(t)$ are the envelopes of the pump and probe pulses, respectively, and the function $N(t) = 1 - \exp(-kt)$, where k is the reaction rate, is used to model product buildup by first-order kinetics. It is worth noting that this form of $N(t)$ is the same as that observed by Schatz and coworkers in trajectory studies of $HOCO^{\dagger}$ decomposition.[38]

To verify the applicability of the rate approach to the present experimental conditions, H_2O_2 was photodissociated via a repulsive potential surface.[46] Such direct dissociation proceeds on the time scale of a vibrational period, which is instantaneous at our present temporal resolution. H_2O_2 photodissociation was used in previous time resolved studies of the CO_2–HI photoinitiated reaction as a measure of the pump–probe cross correlation.[35,36] For instantaneous photodissociation, $N(t)$ is equal to the Heaviside step function, and the signal is given by

$$S(t) = \text{const} \times \int_{-\infty}^{t} ds R_I(s). \tag{5}$$

Fits of the H_2O_2 LIF signals versus pump–probe delay by Eq. (5) are quite satisfactory, as is evident from Fig. 7.

We also measured rates with longer pulses (i.e., ~ 1.2 ps) having narrower spectral widths (i.e., ~ 30 cm^{-1}). These were obtained by replacing the single-plate birefringent filter, which serves as a tuning element in the dye laser, by a two-plate filter. In the presence of coherent effects, deconvoluted "rates" obtained by using Eqs. (3) and (4) depend on pulse durations.[47–51] However, within

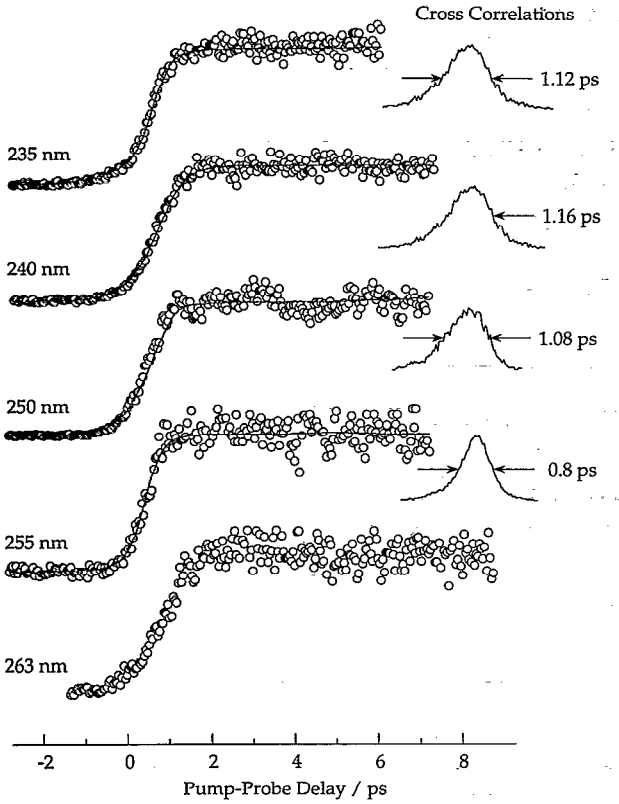

FIG. 7. Hydrogen peroxide photodissociation, details as per Fig. 4.

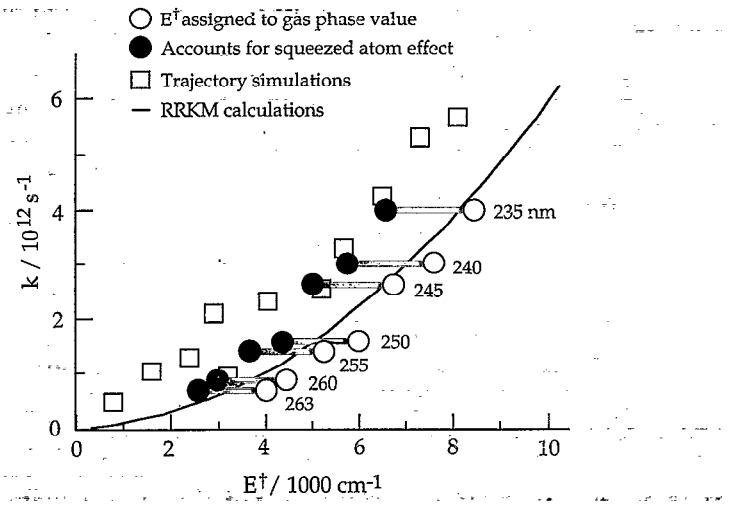

FIG. 8. The circles represent measured reaction rates at the indicated pump wavelengths. Open circles correspond to $E^{\dagger}=E^{\dagger}_{\text{bulk}}$; solid circles represent an attempt to account for the squeezed atom effect: $E^{\dagger}=0.89(E^{\dagger}_{\text{bulk}}+\Delta H)-\Delta H$ (see text). The horizontal lines connecting the circles are for visual convenience. Also shown are the results of RRKM calculations (solid line) (Ref. 33) and the trajectory studies of Schatz and co-workers (squares) (Ref. 38).

the experimental uncertainties, the longer pulses yielded the same reaction rates as those obtained when using shorter ones.

The solid lines in Fig. 4 are best fits of the data by using Eq. (3). Experimental cross correlations were employed and k was the adjustable parameter. For $\lambda_{\text{pump}}=260$ nm, the data were first corrected to account for the spurious transient described in the previous section. This is expected to introduce additional uncertainty. However, rates from three independent scans were quite reproducible: 0.83, 0.93, and 0.91×10^{12} s^{-1}. At $\lambda_{\text{pump}}=263$ nm, we lacked sufficient difference frequency signals to measure reliable cross correlations. In this case, $R_I(s)$ was obtained by differentiating numerically the H_2O_2 signals, i.e., $R_I=dS(t)/dt$ [cf. Eq. (5)].

B. Reaction rates and comparisons to other studies

The rates shown in Fig. 8 were obtained by averaging 3–7 individual fits. Although estimating experimental uncertainties is subjective, we believe that $\pm30\%$ is conservative. OH is produced with a characteristic time—the single exponential risetime $\tau=k^{-1}$ given by Eq. (3)—that is subpicosecond over most of the 235–263 nm photolysis range. This is to be expected on the basis of RRKM calculations.[33]

In contrast to photoinitiated reactions in the gas phase, where there is a one-to-one correspondence between λ_{pump} and the collision energy, there is no rigorous way to assign the internal energy of the $HOCO^{\dagger}$ intermediate for photoinitiated reactions in CO_2–HI complexes. The amount of c.m. translational energy shared between I and HOCO is not clear *a priori*. The open circles in Fig. 8 represent the experimental rates plotted against the HOCO internal energies of the corresponding single collision bulk reactions, i.e.,

$$E^{\dagger}_{\text{bulk}}=(M_I/M_{HI})(M_{CO_2}/M_{HOCO})[h\nu_{\text{pump}}-D_0(HI)]-\Delta H, \quad (6)$$

where $E^{\dagger}_{\text{bulk}}$ is the energy in excess of reaction threshold for bulk conditions; $\Delta H\approx8960$ cm^{-1} is the endothermicity of reaction (1), $D_0(HI)=24\,630$ cm^{-1} is the HI bond energy,[45] and M_X/M_Y is the mass ratio of the indicated species. Note that the I* channel from HI photodissociation is neglected, since the corresponding low energy hydrogen atoms do not react.

For photoinitiated reactions in complexes, Eq. (6) gives the upper limit for $E^{\dagger}$. This is explained in detail elsewhere.[30,33] Briefly, the hydrogen atom that is being photodetached from the iodine finds itself squeezed between the CO_2 and the iodine and, as a result, exerts additional repulsion on the two heavier species. This is borne out in calculations for Ar–HCl complexes[55] and in experiments and calculations for Ar–HBr complexes.[56] It remains to be seen how large the effect is for CO_2–HI, where a reactive window opens and takes in the hydrogen. To get an idea of how large this squeezed atom effect might be, we draw upon earlier $E^{\dagger}$ estimates based on analyses of product state distributions. For 239 nm, CO_2–HI photolysis, a maximal entropy analysis of OH rotational distributions suggested a bimodal distribution of $E^{\dagger}$ values: $\sim30\%$ at ~1000 cm^{-1} and $\sim70\%$ at ~6000 cm^{-1}.[33] The corresponding single collision $E^{\dagger}$ value is approximately 7900 cm^{-1}. The bimodal nature of the $E^{\dagger}$ distributions was nec-

essary to fit the data, but the fits were not sensitive to the exact locations and/or widths of the two $E^\dagger$ clumps. The peak at 6000 cm^{-1} was interpreted as due to the squeezed atom effect, as if the collision energy of 16 900 cm^{-1} had been dropped by 1900 cm^{-1}, an 11% decrease. The ~1000 cm^{-1} peak was thought to be due to another mechanism, perhaps higher-than-binary complexes and/or exit channel interactions with the nearby I atom. Similar analyses for CO_2–HBr yielded ~25% at $E^\dagger \sim 2000$ cm^{-1} and ~75% at $E^\dagger \sim 9000$ cm^{-1}, the latter corresponding to a 12.5% drop in the collision energy.[57]

The solid circles in Fig. 8 represent an attempt to account for the squeezed atom effect by plotting measured rates versus the quantities $0.89\ (E^\dagger_{\text{bulk}}+\Delta H)-\Delta H$, where $E^\dagger_{\text{bulk}}$ is from Eq. (6). It is worth mentioning that the maximal entropy estimations of $E^\dagger$ rely on two assumptions: (i) the halogen atom does not participate in energy redistribution following $HOCO^\dagger$ decomposition, and (ii) unimolecular decomposition governs product state distributions. While the latter is likely to hold, the former is questionable in view of the fast reaction rates. Indeed, the I—HOCO distance increases by only ~1 Å during the 0.3 ps lifetime of the $HOCO^\dagger$ intermediate, so interactions involving all five atoms may occur. Since there are more degrees of freedom in the five-atom system than in HOCO, this can result in OH with less excitation than in the counterpart gas phase reaction. Consequently, the maximal entropy analysis may underestimate $E^\dagger$, making the open and solid symbols in Fig. 8 upper and lower limits, respectively.

The rates presented here are larger than those reported earlier. The same general technique was used but with longer (~5 ps), transform limited, Gaussian pulses.[35,36] When coherent radiation is used to probe chemical dynamics involving long-lived intermediates, the temporal dependence is given by

$$S(t) \propto \int_{-\infty}^{t} dy\{1-\exp[-k(t-y)]\}|R_E(y)|^2, \quad (7)$$

where

$$R_E(y) = \int_{-\infty}^{\infty} dx E_{\text{probe}}(x-y)E_{\text{pump}}(x) \quad (8)$$

is an amplitude cross correlation.[58] These equations differ from Eqs. (3) and(4). However, for Gaussian pulses, $|R_E(t)|^2 \equiv R_I(t)$, and both cases yield identical results. Although effects due to coherence thus appears to be minimal, it is noted that our analysis relies on a two-level approximation. This is reasonable (i) when a single OH transition is excited and (ii) when the whole OH rotational band is excited (which is close to our conditions) and the phases of different OH rotational states are uncorrelated, as is expected for long-lived intermediates. In the present experiments, a number of OH rotational states with $\langle N\rangle \sim 5.5$ are excited by the broadband probe pulse. On the other hand, Scherer *et al.* probed mainly $N=1$, although three points were obtained for $N=6$. Indeed, they found that HOCO lifetimes obtained by monitoring $N=6$ were shorter than those for $N=1$. It may be that the different OH levels hold an important clue. This is being pursued and will be discussed in detail later.[40]

If photoinitiated reactions in higher-than-binary complexes display relatively slow rates, the presence of these species would cause risetimes to appear long and/or bimodal. We therefore searched for a slowly rising component of $S(t)$. None was found (within ±5% uncertainty) over the interval 0–40 ps.

Interestingly, the rates obtained by using complexes are in agreement with RRKM estimates using $E^\dagger$ values near those of the corresponding single collision experiment, while OH rotational distributions are colder than under single collision conditions. The complex environment apparently influences the rates less than the OH rotational distributions. Modest perturbations can disturb product rotations, while stronger interactions are needed to alter HOCO intramolecular dynamics. Perhaps, the interaction between the iodine atom and the HOCO complex is not sufficient for the latter, while OH—I exit channel interactions are sufficient to cool OH rotations.

C. Comparisons with theory

RRKM theory predicts the rates shown as the solid curve in Fig. 8. These calculations used parameters that were obtained by fitting thermal rates over the range $300 \leqslant T \leqslant 2000$ K. From this point of view, our experimental results are in good agreement with the thermal rate data. Figure 8 also shows rates obtained by Schatz and co-workers who studied classical trajectories on the best available potential energy surface.[38] These results agree, albeit roughly, with our measurements. Agreement is also found with the recent quantum scattering calculations of Clary and co-workers (not shown).[41] Thus, it appears that the present results are in reasonable accord, at least for the moment, with theoretical models.

V. CONCLUSIONS

The rates reported herein were obtained under conditions that minimize coherent effects, thereby making them appropriate for comparisons to rate theories and measurements. They are in agreement with results from crossed molecular beams experiments as well as with RRKM calculations and trajectory simulations. Agreement with quantum scattering calculations is reasonable, although this work is still in its preliminary stages.

The HOCO system is an important prototype and will benefit from additional work, such as direct spectroscopic and OH buildup measurements in the threshold region just above D_0(OH–CO). Below D_0(OH–CO), spectroscopic studies of HOCO and time and state resolved dynamics studies of the $H+CO_2$ reactive channel will prove revealing.

ACKNOWLEDGMENTS

We have benefited greatly from discussions with H. Reisler, S. A. Reid, A. H. Zewail, and N. Scherer. Research supported by the National Science Foundation.

[1] P. M. Banks and G. Kocharts, *Aeronomy* (Academic, New York, 1973), p. 362.
[2] I. W. M. Smith and R. Zellner, J. Chem. Soc. Faraday Trans. II **69**, 1617 (1973), and references cited therein.
[3] W. B. DeMore, D. M. Golden, R. F. Hampson, Jr., C. J. Howard, M. J. Kurylo, M. J. Molina, A. R. Ravishankar, and S. P. Sander (unpublished).
[4] J. Warnatz, in *Combustion Chemistry*, edited by W. C. Gardiner, Jr. (Springer-Verlag, New York, 1984), p. 197.
[5] J. A. Miller and G. A. Fisk, Chem. Eng. News **65**, 22 (1987).
[6] D. L. Baulch and D. D. Drysdale, Combust. Flame **23**, 215 (1974).
[7] C. D. Jonah, W. A. Mulac, and P. Zeglinski, J. Phys. Chem. **88**, 4100 (1984).
[8] D. L. Baulch, R. A. Cox, R. F. Hampson, Jr., J. A. Kerr, J. Troe, and R. T. Watson, J. Phys. Chem. Ref. Data **13**, 1259 (1984).
[9] R. R. Ravishankara and R. L. Thompson, Chem. Phys. Lett. **99**, 377 (1983).
[10] J. Brunning, D. W. Derbyshire, I. W. M. Smith, and M. D. Williams, J. Chem. Soc. Faraday Trans. II **84**, 105 (1988).
[11] M. J. Frost, P. Sharkey, and I. W. M. Smith, Faraday Discuss. Chem. Soc. **91**, 305 (1991).
[12] (a) D. E. Milligan and Jacox, J. Chem. Phys. **54**, 927 (1971); (b) H. E. Radford, W. Wei, and T. J. Sears, *ibid.* **97**, 3989 (1992); (c) T. J. Sears, H. E. Radford, and M. A. Moore, *ibid.* **98**, 6624 (1993); (d) J. T. Petty and C. B. Moore (unpublished).
[13] J. C. Schatz, M. S. Fitzcharles, and L. B. Harding, Faraday Discuss. Chem. Soc. **84**, 359 (1987).
[14] G. A. Oldershaw and D. A. Porter, Nature **223**, 490 (1969).
[15] R. E. Tomalesky and J. E. Sturm, J. Chem. Soc. Faraday Trans. II **68**, 1241 (1972).
[16] C. R. Quick, Jr., R. E. Weston, Jr., and G. W. Flynn, Chem. Phys. Lett. **83**, 15 (1981).
[17] Y. Chen, G. Hoffmann, D. Oh, and C. Wittig, Chem. Phys. Lett. **159**, 426 (1989).
[18] C. Wittig, G. Hoffmann, Y. Chen, H. Iams, and D. Oh, J. Chem. Soc. Faraday Trans. II **85**, 1292 (1989).
[19] K. Kleinermanns and J. Wolfrum, Laser Chem. **2**, 339 (1983).
[20] K. Kleinermanns and J. Wolfrum, Chem. Phys. Lett. **104**, 157 (1984).
[21] K. Kleinermanns, E. Linnebach, and J. Wolfrum, J. Phys. Chem. **89**, 2525 (1985).
[22] A. Jacobs, M. Wahl, R. Weller, and J. Wolfrum, Chem. Phys. Lett. **158**, 161 (1989).
[23] J. Wolfrum (private communication).
[24] S. Nickolaisen, H. E. Cartland, and C. Wittig, J. Chem. Phys. **96**, 4378 (1992).
[25] J. K. Rice, Y. C. Chung, and A. P. Baronavski, Chem. Phys. Lett. **167**, 151 (1990).
[26] S. K. Shin, Y. Chen, S. Nickolaisen, S. W. Sharpe, R. A. Beaudet, and C. Wittig, in *Advances in Photochemistry*, edited by D. Volman, G. Hammond, and D. Neckers (Wiley, New York, 1991), Vol. 16, p. 249.
[27] F. A. Baiocchi, T. A. Dixon, C. H. Joyner, and W. Klemperer, J. Chem. Phys. **74**, 6544 (1981).
[28] R. S. Altman, M. S. Marshall, and W. Klemperer, J. Chem. Phys. **77**, 4344 (1982).
[29] S. W. Sharpe, Y. P. Zeng, C. Wittig, and R. A. Beaudet, J. Chem. Phys. **92**, 943 (1990).
[30] Y. Chen, G. Hoffmann, S. K. Shin, D. Oh, S. Sharpe, Y. P. Zeng, R. A. Beaudet, and C. Wittig, in *Advances in Molecular Vibrations and Collision Dynamics* (JAI Press, Greenwich, 1992), Vol. 1, p. 187.
[31] Y. P. Zeng, S. W. Sharpe, S. K. Shin, C. Wittig, and R. A. Beaudet, J. Chem. Phys. **97**, 5392 (1992).
[32] S. K. Shin, Y. Chen, D. Oh, and C. Wittig, Philos. Trans. R. Soc. London Ser. A **332**, 361 (1990).
[33] G. Hoffmann, D. Oh, Y. Chen, Y. M. Engel, and C. Wittig, Israel J. Chem. **30**, 115 (1990).
[34] S. K. Shin, C. Wittig, and W. A. Goddard III, J. Phys. Chem. **95**, 8048 (1991).
[35] N. F. Scherer, L. R. Khundkar, R. B. Bernstein, and A. H. Zewail, J. Chem. Phys. **87**, 1451 (1987).
[36] N. F. Scherer, C. Sipes, R. B. Bernstein, and A. H. Zewail, J. Chem. Phys. **92**, 5239 (1990).
[37] M. Alagia, N. Balucani, and P. Casavecchia, J. Chem. Phys. (to be published).
[38] K. Kudla, G. C. Schatz, and A. F. Wagner, J. Chem. Phys. **95**, 1635 (1991).
[39] S. I. Ionov, G. A. Brucker, C. Jaques, L. Valachovic, and C. Wittig, J. Chem. Phys. **97**, 9486 (1992).
[40] S. I. Ionov, C. Wittig, and A. H. Zewail (unpublished).
[41] D. C. Clary, Conference of Orientation and Polarization Effects in Chemical Reaction Dynamics, Perugia, Italy, November, 1992, paper 36.
[42] S. I. Ionov, G. A. Brucker, C. Jaques, Y. Chen, and C. Wittig, J. Chem. Phys. **99**, 3420 (1993).
[43] O. E. Martinez, IEEE J. Quantum Electron. **QE-23**, 59 (1987).
[44] T. E. Sharp, C. B. Dane, D. Barber, F. K. Tittel, P. J. Wisoff, and G. Szabo, IEEE J. Quantum Electron. **QE-27**, 1221 (1991).
[45] K. P. Huber and G. Herzberg, *Molecular Spectra and Molecular Structure. IV. Constants of Diatomic Molecules* (Van Nostrand Reinhold Co., New York, 1979).
[46] H. Okabe, *Photochemistry of Small Molecules* (Wiley, New York, 1978).
[47] S. O. Williams and D. G. Imre, J. Phys. Chem. **92**, 6636 (1988); **92**, 6648 (1988).
[48] J. L. Krause, M. Shapiro, and R. Bersohn, J. Chem. Phys. **94**, 5499 (1991).
[49] R. Heather and H. Metiu, Chem. Phys. Lett. **157**, 505 (1989).
[50] R. B. Bavil, V. Engel, and H. Metiu, J. Chem. Phys. **96**, 2600 (1992).
[51] H. Metiu, Faraday Discuss. Chem. Soc. **91**, 249 (1991).
[52] P. M. Felker, J. S. Baskin, and A. H. Zewail, J. Phys. Chem. **90**, 724 (1986); J. S. Baskin, P. M. Felker, and A. H. Zewail, J. Chem. Phys. **84**, 4708 (1986).
[53] P. M. Felker and A. H. Zewail, J. Chem. Phys. **86**, 2460 (1987); J. S. Baskin, P. M. Felker, and A. H. Zewail, *ibid.* **86**, 2483 (1987).
[54] For a review of current activity in the field, see P. M. Felker, J. Phys. Chem. **96**, 7844 (1992), and references cited therein.
[55] A. Garcia-Vela, R. B. Gerber, and J. J. Valentini, Chem. Phys. Lett. **186**, 223 (1991); J. Chem. Phys. **97**, 3297 (1992).
[56] J. Segall, Y. Wen, R. Singer, C. Wittig, A. Garcia-Vela, and R. B. Gerber, Chem. Phys. Lett. **207**, 504 (1993).
[57] C. Wittig, Y. M. Engel, and R. D. Levine, Chem. Phys. Lett. **153**, 411 (1988).
[58] S. I. Ionov and C. Wittig (unpublished).